ScienceDirect
IFAC PapersOnLine 51-29 (2018) 62–67
IFAC Papers Online
CONFERENCE PAPER ARCHIVE

Wave Energy Control Systems: Robustness Issues ⋆

John V. Ringwood * **Alexis Merigaud** * **Nicolás Faedo** *
Francesco Fusco **
* *Centre for Ocean Energy Research, Maynooth University, Co. Kildare, Ireland (e-mail: john.ringwood@mu.ie).*
** *Smarter Cities Technology Centre, IBM Research Ireland, Mulhuddart, Dublin 15, Ireland (e-mail: francfus@ie.ibm.com)*

Abstract: While traditional feedback control systems enjoy relatively good sensitivity properties, energy maximising wave energy converter (WEC) control systems have particular characteristics which challenge the application of traditional feedback and robust control methods. In particular, the relationship between plant and controller is largely defined by the need to maximise power transfer, and the controller contains a feedforward component which is difficult to robustify. Typically, WEC control systems are based on linear model descriptions, but this belies the true nonlinearity of WEC hydrodynamics (particularly under controlled conditions) and the associated power take-off (PTO) system. This paper examines two popular WEC control structures and examines the sensitivity of these structures to parameter variations, both in terms of closed-loop transfer functions and power absorbed. Some recommendations are also given on which WEC parameters need to be modelled with high accuracy.

Keywords: Wave energy, control system, sensitivity, robustness, power maximisation

1. INTRODUCTION

The vast majority of WEC control strategies are model-based and rely on a hydrodynamic model, which describes the mathematical relationship between the incident waves and the mechanical response of the WEC. However, it is not clear how *robust* model-based WEC control systems are to modelling errors. A variety of reasons exist why modelling errors are potentially significant in current model-based WEC control strategies. Linear hydrodynamic theory is challenged, particularly in relation to small movements around the equilibrium position. Also, model-based control strategies must run in real-time, therefore limiting the computational complexity of the hydrodynamic models employed. In particular, there is a limit to the complexity of hydrodynamic model for which an optimal control solution can be found, either algebraically or numerically. In addition, many WEC hydrodynamic models are validated in tank tests where the excitation is provided only through variation in the free-surface elevation with no external PTO force present, limiting variations in wetted surface. Finally, WEC controllers are often validated in simulation using the exact model upon which the controller was determined, thus masking any sensitivity issues.

While it is well known that the closed-loop sensitivity of traditional servo/regulatory control loops is enhanced through feedback control, this is not necessarily the case for energy maximising control systems, since many WEC controllers contain a feedforward part, and the energy maximising control objective leads to a very specific relationship between controller and plant, preventing the use of high gain to reduce sensitivity.

While a small number of studies have developed robust controllers for aspects of the WEC control problem (e.g. Fusco and Ringwood (2014); OSullivan and Lightbody (2017)), a detailed overview of the broad sensitivity and robustness issues associated with WEC controllers has been missing.

2. WEC MODELS AND CONTROL STRUCTURES

2.1 WEC models for model-based control

For simplicity, we consider a single-body floating system oscillating in heave, schematically depicted in Fig.1. Energy is extracted from the relative motion with the sea bottom, through a generic PTO mechanism. The external forces acting on the WEC are the excitation from the waves and the control force produced by the PTO, namely $f_{ex}(t)$ and $f_{PTO}(t)$, respectively.

Ignoring any mooring or viscous damping forces results in the widely used Cummins' equation (Cummins, 1962),

$$(M + m_\infty)\dot{v}(t) + \int_0^{+\infty} h_r(\tau)v(t-\tau)d\tau + kx(t) = \int_{-\infty}^{t} h_{ex}(\tau)\eta(t-\tau)d\tau + f_{PTO}(t). \quad (1)$$

where $v(t)$ is the heave velocity, M the WEC mass, and k the restoring force spring constant. h_r and h_{ex} are hydrodynamic parameters related to the radiation

⋆ This work was supported by Science Foundation Ireland under Grant No. SFI/13/IA/1886 and Grant No. 12/RC/2302 for the Marine Renewable Ireland (MaREI) centre.

10.1016/j.ifacol.2018.09.470

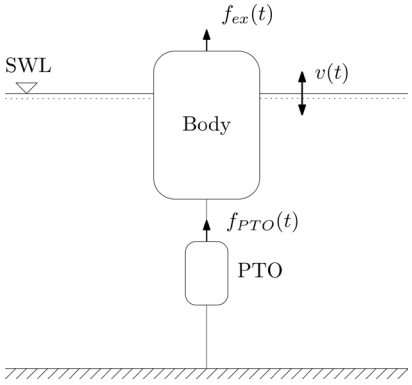

Fig. 1. One-degree-of-freedom floating system for wave-energy conversion, with the lower side of the PTO anchored to the sea bed.

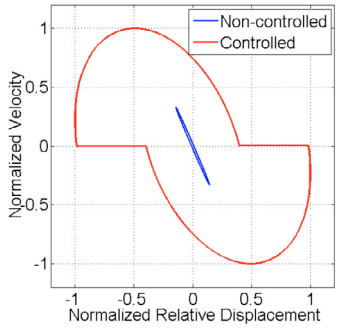

Fig. 2. Operational space covered by an uncontrolled and controlled spherical heaving buoy

damping and excitation forces, respectively. The model in (1), widespread in WEC control studies, has the following limitations:

(1) There is an assumption that the device experiences small oscillations, while the objective, in maximum energy capture, is to exaggerate motion.
(2) Viscous effects are ignored.
(3) Linear excitation and buoyancy forces are only reasonable when the oscillating body has a uniform cross-sectional area (Giorgi and Ringwood, 2017).

In addition, WEC models, determined under uncontrolled conditions are probably not representative, with Fig.2 showing the operational space (in terms of velocity and displacement) covered by an uncontrolled and a (latching) controlled spherical heaving buoy (Giorgi et al., 2016). Under controlled conditions, there are increases in viscous effects (due to relative device/fluid velocity) and nonlinear Froude-Krylov (excitation/buoyancy) forces (due to increases in the wetted surface variation).

Finally, there are also likely to be (at least) minor inaccuracies in the determination of $h_r(\tau)$, m_∞ via mesh-based linear boundary element solvers, due to discretization of the domain, and other effects. Overall, then, there is likely to to a significant disparity between the real WEC dynamics and those represented by (1), typically used for model-based controller development. However, these system/controller mismatch issues are frequently masked by the employment of a simulation/evaluation model which is also based on (1), which tends to be relatively common practice in WEC control studies.

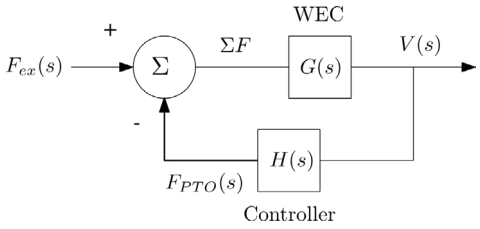

Fig. 3. ACC controller structure, which directly calculates the PTO force, using (4)

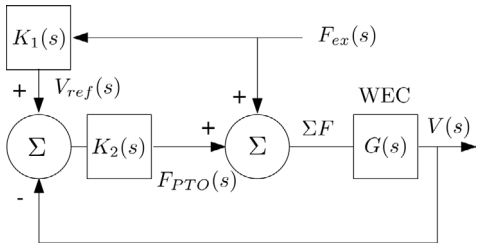

Fig. 4. AVT controller structure, which calculates the optimal velocity profile, prior to the use of a tracking control loop to achieve that velocity profile

2.2 WEC control structures

WEC controllers are employed to maximise converted wave power. Considering the frequency-domain equivalent of (1), namely

$$\frac{V(\omega)}{F_{ex}(\omega)+F_{PTO}(\omega)} = \frac{1}{Z_i(\omega)}, \tag{2}$$

where $Z_i(\omega)$ is the intrinsic WEC impedance:

$$Z_i(\omega) = B_r(\omega) + \jmath\omega\left[M + M_a(\omega) - \frac{k}{\omega^2}\right], \tag{3}$$

with $M_a(\omega)$ the added mass ($m_\infty - \lim_{\omega\to\infty} M_a(\omega)$ and $B_r(\omega)$ the radiation damping.

For maximum power transfer, we choose a controller 'impedance' $Z_c(\omega)$, ($F_{PTO} = Z_c V$), so that

$$Z_c(\omega) = Z_i^*(\omega), \tag{4}$$

where z^* denotes the complex conjugate of $z \in \mathbb{C}$. Alternatively, an optimal velocity profile $V_{opt}(\omega)$ to follow can be generated (Falnes, 2002) as:

$$V_{opt}(\omega) = \frac{F_{ex}(\omega)}{2R_i(\omega)} \tag{5}$$

where $R_i = 1/2\ (Z_i + Z_i^*)$ is the real part of Z_i. Equations (4) and (5) essentially lead to the two fundamental WEC controller configurations:

(1) The ACC structure, and
(2) The AVT structure,

following the designation of Hals et al. (2011). The ACC controller, which directly produces a power take-off (PTO) force input from measurment of device velocity, is shown in Fig.3, while the AVT controller, which first calculates the optimal velocity trajectory, and subsequently implements a tracking control loop to follow that trajectory, is shown in Fig.4.

The various components of the ACC and AVT controllers are defined, in the Laplace domain, as follows:

$G(s)$ is the linear WEC model, which defines the velocity $V(s)$ resulting from the application of a combination of excitation force $F_{ex}(s)$ and PTO force $F_{PTO}(s)$,
$H(s)$ is the direct force WEC controller,
$K_1(s)$ is the velocity setpoint calculation, based on the excitation force F_{ex}, and
$K_2(s)$ is the feedback controller which tries to maintain the WEC velocity profile at its setpoint.

We note that $G(s)$ contains finite-order linear dynamic approximations to the non-parametric impulse response excitation force ($h_r(t)$) and radiation damping (h_{ex}) kernels that typically result from the hydrodynamic parameters calculated using boundary-element methods, such as WAMIT or NEMOH.

In the ACC controller, the control force is suitably parameterised as:

$$f_{PTO}(t) = M_c\ddot{x}(t) + B_c\dot{x}(t) + k_c x(t), \tag{6}$$

giving

$$Z_c = B_c + j\left(\omega M_c - \frac{k_c}{\omega}\right), \tag{7}$$

and $H(s)$ represents the Laplace equivalent of $Z_c(\omega)$.

Three controller parameter choices all achieve the required complex conjugate (Hansen, 2013), since the 3-term controller (8) has, effectively, one redundant term, since only a combination which yields a single real and imaginary term is required to achieve the condition in (4)

$$M_c(\omega) = -\left(M + M_a(\omega)\right), \qquad k_c = k, \;\; B_c = B_r. \tag{8}$$

For the AVT case, the controller is not so easily parameterised, but uses a direct implementation of (5). Some notes on these basic controller configurations are appropriate at this point.

Both (4) and (5) are functions of frequency ω, indicating that either only a single wave frequency is handled, or that the controller parameters must be adapted with frequency. In practice, a panchromatic version of the ACC controller has been developed (Nielsen et al., 2013), while $v_{ref}(t)$, in the AVT controller, is usually evaluated as the solution of a numerical optimisation problem (Faedo et al., 2017).

As in many other applications, it is important that key variables (displacement, velocity, force) are kept within physical limits. While the basic calculations in (4) and (5) ignore physical constraints, constrained optimisation can be used (Faedo et al., 2017) to ensure physical constraints are met. In general, constrained solutions for the ACC controller are not yet available.

Since $h_r(t)$ is causal, $h_c(t) = \mathcal{F}^{-1}\{Z_c(\omega)\}$ (inverse Fourier transform of Z_c) is anticausal, requiring future knowledge of the excitation force. While this knowledge is straightforward for the monochromatic case (single sinusoid), it is more problematic for irregular seas. The issue of forecasting random seas is dealt with by Fusco and Ringwood (2010). We note that, since it is based on instantaneous velocity feedback, the simpler ACC controller has the advantage that it does not require future values of the excitation force. However, a suboptimal causal solution is required, for the panchromatic case, as a result (Nielsen et al., 2013).

The issues outlined above significantly complicate any robustness/sensitivity analysis. As a consequence, where possible, we will assume perfect future knowledge of f_{ex}, though some consideration to errors in f_{ex} will be given in Section 3, while a more thorough treatment of the effects of f_{ex} forecast errors is given by Fusco and Ringwood (2011a). For the present, physical constraints will be addressed in a somewhat qualitative way.

3. SOME SENSITIVITY CALCULATIONS

3.1 Sensitivity functions

In this section, we determine the sensitivity of the overall closed-loop transfer function (CLTF), $T(s) = V(s)/F_{ex}(s)$, to variations in the WEC model, $G(s)$.

3.2 ACC Structure

The transfer functions of the WEC device $G(s)$, and the complex conjugate controller $H(s)$, are given, respectively, by

$$G(s) = \frac{s}{(M + M_a^\omega)s^2 + B_r^\omega s + k}, \tag{9}$$

$$H(s) = \frac{-(M + M_a^\omega)s^2 + B_r^\omega s - k}{s}, \tag{10}$$

where $B_r^\omega = B_r(\omega)$ and $M_a^\omega = M_a(\omega)$, to simplify the notation. With the definition of $G(s)$ in (9) and $H(s)$ in (10), the closed-loop transfer function $T(s)$, from the reference input $F_{ex}(s)$ to the output $V(s)$, is

$$T(s) = \frac{G(s)}{1 + G(s)H(s)} = \frac{1}{2B_r^\omega}, \tag{11}$$

where B_r^ω is real and even. As expected, the ACC controller achieves the well-known optimal velocity profile (Falnes, 2002), expressed as

$$V(s) = T(s)F_{ex}(s) = \frac{F_{ex}(s)}{2B_r^\omega}. \tag{12}$$

Since the controller (10) is based on a simplified model of the real process, the sensitivity of the closed-loop transfer function $T(s)$ (11) to variations in the open-loop transfer function $G(s)$ (9), is important for performance analysis of the ACC loop under realistic conditions. The classical definition of a *sensitivity function* $S_G^T(s)$ provides a measure of how sensitive the closed-loop transfer function $T(s)$ is to small variations in $G(s)$, namely

$$S_G^T(s) = \frac{dT(s)}{dG(s)}\frac{G(s)}{T(s)} = \frac{1}{1 + G(s)H(s)}. \tag{13}$$

If $\left|S_G^T(s)\right| < 1$, the percentage change in $T(s)$ is less than the percentage change in $G(s)$, indicating a sensitivity improvement. Considering (13), and using (9) and (10), the sensitivity funcion for the ACC loop is given by

$$S_G^T(s) = \frac{(M + M_a^\omega)s^2 + B_r^\omega s + k}{2B_r^\omega s}. \tag{14}$$

Fig.5 depicts $\left|S_G^T(\omega)\right|$ for the example cylindrical WEC. Note that the ACC structure is extremely sensitive to variations in $G(s)$, increasing for frequencies away from the device resonant frequency $\omega_r \approx \sqrt{k/(M + m_\infty)} \approx 0.67$ rads/s, where $|S_G^T| = 0.5$.

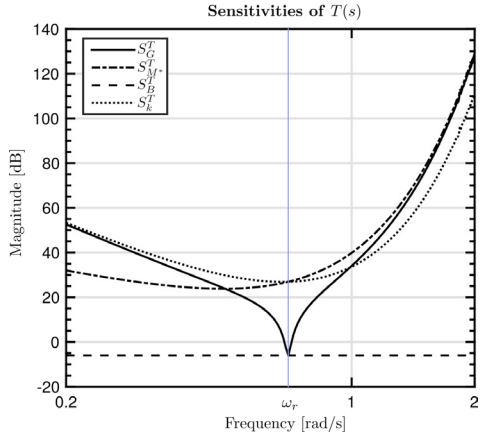

Fig. 5. Sensitivity functions for the ACC control loop. The vertical line shows the resonant frequency ω_r.

We can also develop explicit expressions for the sensitivity of the closed-loop transfer function $T(s)$ to each hydrodynamic parameter separately. The general definition for the sensitivity of $T(s)$ to a specific parameter α is given by

$$S_\alpha^T(s) = \frac{\alpha}{T(s)}\frac{dT(s)}{d\alpha} = S_G^T(s)S_\alpha^G(s), \tag{15}$$

where $S_\alpha^G(s)$ denotes the sensitivity of the open-loop transfer function $G(s)$ to variations in α. Defining $M^* = M + M_a^\omega$, the sensitivity of $G(s)$ to each parameter M^*, B_r^ω and k, can be independently evaluated as

$$S_{M^*}^G(s) = -\frac{M^*s^2}{M^*s^2 + B_r^\omega s + k}, \tag{16}$$

$$S_B^G(s) = -\frac{B_r^\omega s}{M^*s^2 + B_r^\omega s + k}, \tag{17}$$

$$S_k^G(s) = -\frac{k}{M^*s^2 + B_r^\omega s + k}. \tag{18}$$

From a traditional 'tracking' control perspective, the controller $H(s)$ should be designed so that $S_G^T(s)$ reduces the open-loop sensitivity to parameter variations (at least in the wave frequency range). However, in the ACC case, S_G^T dramatically *amplifies* the sensitivities defined in (16), (17) and (18) at almost all frequencies, except near ω_r, where the sensitivity magnitude is reduced (maximally) by a factor of 2. The sensitivities of $T(s)$ to variations in M^*, B_r^ω and k, from (15), are:

$$S_{M^*}^T(s) = S_G^T(s)S_{M^*}^G(s) = -\frac{M^*s^2}{2B_r^\omega}, \tag{19}$$

$$S_B^T(s) = S_G^T(s)S_B^G(s) = -\frac{1}{2}, \tag{20}$$

$$S_K^T(s) = S_G^T(s)S_K^G(s) = -\frac{k}{2B_r^\omega s}. \tag{21}$$

and are plotted in Fig.5, along with $S_G^T(s)$.

3.3 AVT Structure

The AVT controller follows into a more traditional feedforward/feedback structure, which is straightforward to analyse. In particular, $S_{K_1}^T(s) = 1$, suggesting that the optimal velocity reference is uniformely sensitive to errors in the calculation of K_1, or whatever other calculation is performed (e.g. see Faedo et al. (2017)) to evaluate the optimal velocity profile. Clearly, some compromise may be achieved so that a 'desensitised' velocity profile might be calculated (e.g. Fusco and Ringwood (2014)) but while this might have positive implications for sensitivity, it is likely to negatively impact performance, to a greater or lesser extent.

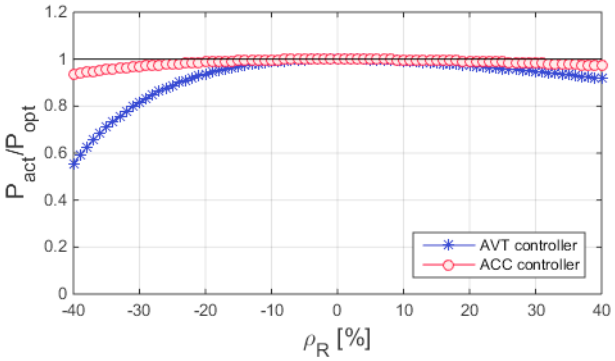

Fig. 6. Sensitivity of power absorption to damping modelling errors

The velocity tracking loop, controlled by K_2, however, is a classical feedback tracking loop and robust control techniques from the broad control systems science area can be applied. A number of examples have been demonstrated in the literature, including an internal model controller, robustified using small gain and/or passivity (Fusco and Ringwood, 2014), backstepping (Genest and Ringwood, 2017), and sliding mode control (Wahyudie et al., 2015).

4. POWER CAPTURE SENSITIVITY

Defining $\rho_\Re := \frac{\Re\{\epsilon_Z\}}{\Re\{Z_i\}}$ as the relative error in the radiation damping term, while $\rho_\Im = \frac{\Im\{\epsilon_Z\}}{\Im\{Z\}}$ represents relative errors in either inertial or stiffness terms, we can now analyse the sensitivity, P_{act}/P^o, to different error types, where P^o is power converted for the nominal system and P_{act} the actual power converted under perturbed conditions.

4.1 ACC structure

With modelling errors on damping terms only, i.e. errors in $\Re\{Z_i\}$, we get (Ringwood et al., 2018):

$$S_\Re(\rho_\Re) = \frac{1+\rho_\Re}{1+\rho_\Re+\frac{1}{4}\rho_\Re^2} \tag{22}$$

which is represented in Fig.6. For $\rho_\Re \ll 1$, developing (22) up to order 2 yields $S_\Re(\rho_\Re) \approx 1 - \frac{1}{4}\rho_\Re^2$. Therefore, $S_\Re(\rho_\Re)$ depends quadratically on the relative error in damping terms. For example, a 10% under- or over-estimation of radiation damping terms only reduces power absorption by approximately 0.25%.

Considering modelling errors in inertial or stiffness terms (i.e. errors in $\Im\{Z_i\}$), we get (Ringwood et al., 2018):

$$S_\Im(\rho_\Im) = \frac{1}{1+\frac{1}{4}\frac{\Im\{Z_i\}^2}{\Re\{Z_i\}^2}\rho_\Im^2} \tag{23}$$

For 7s, 9s and 12s wave periods (equivalent to angular frequencies of 0.9, 0.7 and 0.52 rads/sec, respectively), the

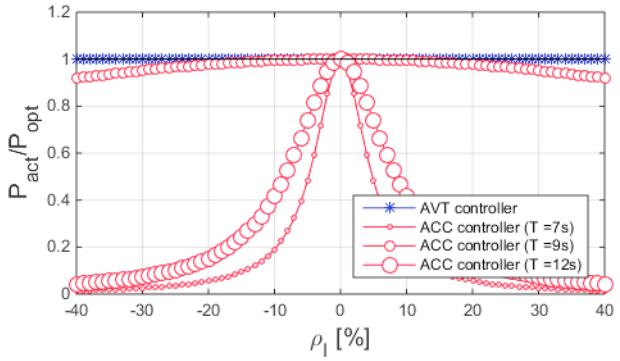

Fig. 7. Sensitivity of power absorption to inertial and stiffness errors in ACC and AVT controllers

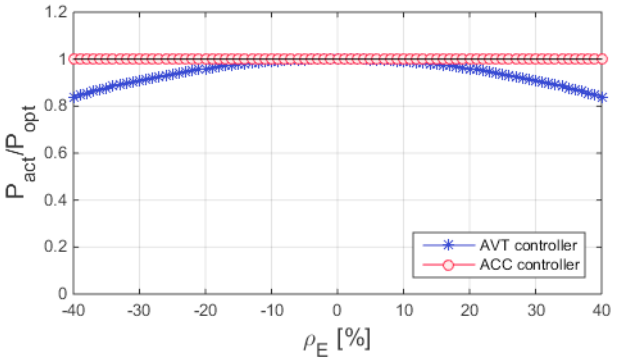

Fig. 8. Sensitivity of power absorption to excitation force modelling errors

power sensitivity (P_{act}/P^o) to errors in inertial or stiffness terms is compared in Fig.7 for AVT and ACC cases. It can be seen that the sensitivity is small for excitation periods in the neighborhood of the device resonant period ($T_{res} \approx 9$s), where the controller is relatively redundant. In contrast, for excitation signal frequencies away from the resonant period, and where the controller is needed, modelling errors have a significant impact on power absorption. For example (see Fig.7); with a wave period of 12s, a relative impedance error level of only 10% results in a 60% drop in the absorbed power, from the matched case. As can be seen in Fig.8, the absorbed power, with the ACC controller, is not affected by errors in the excitation force.

4.2 AVT structure

The sensitivity of extracted power to damping error is (Ringwood et al., 2018):

$$S_{\Re}(\rho_{\Re}) := \frac{P_{act}}{P^o} = \frac{1+2\rho_{\Re}}{(1+\rho_{\Re})^2} \tag{24}$$

The function $S_{\Re}(\rho_{\Re})$ is clearly frequency independent, and is plotted in Fig.6. Assuming $\rho_{\Re} \ll 1$, and developing (24) up to order 2, yields $S_{\Re}(\rho_{\Re}) \approx 1-\rho_{\Re}^2$. Therefore, for small errors in radiation damping, the loss in power production evolves quadratically with the relative error: A 10% over- or under-estimation of damping terms results in a loss of approximately 1% in power extraction.

Considered over a wider range of error values, the sensitivity function in (24) is not symmetric with respect to the sign of the error. More precisely, overestimation of radiation damping terms has a relatively small impact on power production, compared to underestimation of the same magnitude, also confirmed by the simulation results in (OSullivan and Lightbody, 2017). For example, overestimating the damping coefficient by 40% results in a power loss of less than 10%. This suggests that the damping term included in the controller should be over-conservative, rather than under-conservative.

We can also note that power absorption, under AVT control, is insensitive to modelling errors in *inertial* and *stiffness* terms, being uniformly equal to one in Fig.7.

Finally, analysing the sensitivity with respect to a relative error in excitation force yields:

$$S_E(\rho_E) = 1 - |\rho_E|^2. \tag{25}$$

$S_E(\rho_E)$ is plotted in Fig.8, for the case where ϵ_E and F_{ex} have the same phase over $[0;\pi]$, i.e. ρ_E takes positive and negative real values. If the excitation force error magnitude is 10 %, power extraction decreases by just 1%.

5. SAMPLE SIMULATION RESULTS

For the numerical results presented in this section, the WEC model considered is a heaving cylinder with 7[m] radius, 20[m] height and 16[m] draft. The hydrodynamic parameters $(M_a(\omega), B_r(\omega), H_{ex}(\omega))$ are calculated using WAMIT.

5.1 Control implementation

AVT control loop The AVT controller of Fig.4 is designed based on the procedure proposed in Fusco and Ringwood (2014). In particular, the velocity setpoint calculation is based on a frequency-dependent proportional law, $K_1(s) = 1/2\,(B(\omega_0))$, where the instantaneous wave frequency ω_0 is adapted in real-time, based on the peak frequency of the excitation force, and estimated with an Extended Kalman Filter (EKF). The nominal feedback controller, $K_2(s)$, is based on the internal model control procedure, as described in (Fusco and Ringwood, 2014).

Two variants of the AVT controller of Fig.4 are implemented. In the first one, simply termed *AVT*, the tracking feedback controller, $K_2(s)$, is based on the nominal model of the WEC. Therefore, any modelling error has an impact on both the reference velocity generation *and* on the tracking loop. In the *robust AVT*, $K_2(s)$ is based on a positive definite approximation of the nominal feedback controller, following the method proposed in (Fusco and Ringwood, 2014).

ACC control loop The feedback law of the ACC controller in Fig 3, $H(s)$, is based on the reciprocal of the complex-conjugate of a second-order approximation of the nominal plant (Fusco and Ringwood, 2011b):

$$H(s) = F(s)/G^*_{eq}(s). \tag{26}$$

An additional band-pass filter $F(s)$ is needed in order to make the controller realisable, $F(s) = 100s/[(s+0.002)\cdot(s+100)]$, with a negligible effect on the system over the typical frequency range of incident waves.

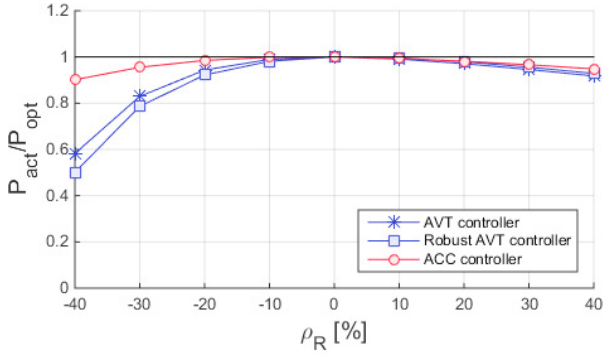

Fig. 9. Simulation results: sensitivity of power absorption to damping term modelling errors. Results are averaged over frequency.

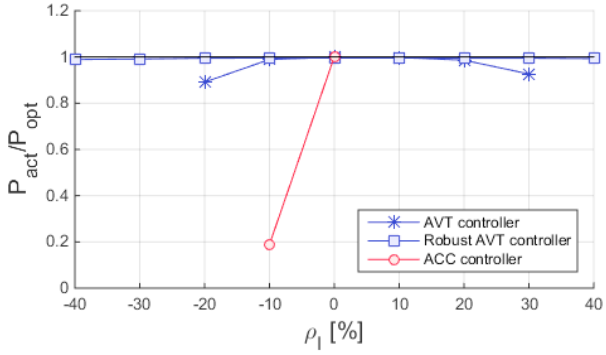

Fig. 10. Simulation results: sensitivity of power absorption to inertial term modelling errors. Missing points indicate cases where the simulation is unstable. Results are averaged over frequency.

5.2 Numerical setup

An excitation force signal was generated from single-peak Ochi spectra with various peak frequencies, and with a significant wave height of $H_s = 1$[m] and $\lambda = 3$, based on the procedure in (Figwer, 1997).

5.3 Simulation results

Errors in radiation damping terms The power absorption sensitivity,calculated as P_{act}/P^o, is shown in Fig.9. For the AVT loop, the sensitivity of power absorption to damping term errors shows the same order of magnitude as predicted by theory (Fig.6), and the same asymmetry with respect to the sign of the error. We can also note that the ACC loop shows a lower sensitivity than AVT to damping errors, as was also the case in Fig.6.

Errors in inertial terms From Fig. 10, for the simple AVT loop, beyond a 20-30% error level, tracking cannot be carried out successfully, and the velocity tracking loop becomes unstable. However, with the robust AVT approach, the trajectory is successfully tracked, in spite of the modelling errors. For the ACC loop, the sensitivity properties are worse than predicted by the theoretical calculations (Fig.7); even small modelling errors have the potential to make the control loop unstable.

REFERENCES

Cummins, W. (1962). The impulse response function and ship motions. *Schiffstechnik*, 9, 101–109.

Faedo, N., Olaya, S., and Ringwood, J.V. (2017). Optimal control, MPC and MPC-like algorithms for wave energy systems: An overview. *IFAC Journal of Systems and Control*.

Falnes, J. (2002). *Ocean waves and oscillating systems: linear interactions including wave-energy extraction*. Cambridge university press.

Figwer, J. (1997). A new method of random time-series simulation. *Sim. Practice and Theory*, 5(3), 217–234.

Fusco, F. and Ringwood, J.V. (2014). Hierarchical robust control of oscillating wave energy converters with uncertain dynamics. *IEEE Transactions on Sustainable Energy*, 5(3), 958–966.

Fusco, F. and Ringwood, J.V. (2010). Short-term wave forecasting for real-time control of wave energy converters. *IEEE Trans. on Sust. Energy*, 1(2), 99–106.

Fusco, F. and Ringwood, J.V. (2011a). A model for the sensitivity of non-causal control of wave energy converters to wave excitation force prediction errors. In *European Wave and Tidal Energy Conference (EWTEC), Southampton*.

Fusco, F. and Ringwood, J.V. (2011b). Suboptimal causal reactive control of wave energy converters using a second order system model. In *Proc. of the 21st Intl. Offshore and Polar Engineering Conf.*, 687–694.

Genest, R. and Ringwood, J.V. (2017). Receding horizon pseudospectral control for energy maximization with application to wave energy devices. *IEEE Transactions on Control Systems Technology*, 25(1), 29–38.

Giorgi, G., Retes, M.P., and Ringwood, J.V. (2016). Comparison of different nonlinear modelling options for heaving buoy wave energy converters. In *Asian and Tidal Energy Conference (AWTEC), Singapore*.

Giorgi, G. and Ringwood, J.V. (2017). Froude-krylov and viscous drag representations in nonlinear wave energy devices models in the computation/fidelity continuum. *Ocean Engineering*, 141, 164–175.

Hals, J., Falnes, J., and Moan, T. (2011). A comparison of selected strategies for adaptive control of wave energy converters. *Journal of Offshore Mechanics and Arctic Engineering*, 133(3), 031101–031113.

Hansen, R. (2013). *Design and control of the power take-off system for a wave energy converter with multiple absorbers*. Ph.D. thesis, Aalborg University.

Nielsen, S.R., Zhou, Q., Kramer, M.M., Basu, B., and Zhang, Z. (2013). Optimal control of nonlinear wave energy point converters. *Ocean Eng.*, 72, 176–187.

OSullivan, A.C. and Lightbody, G. (2017). The effect of viscosity on the maximisation of electrical power from a wave energy converter under predictive control. *IFAC-PapersOnLine*, 50(1), 14698–14704.

Ringwood, John V andMerigaud, A., Faedo, N., and Fusco, F. (2018). On the sensitivity and robustness of wave energy control systems. *IEEE Trans. on Control Systems Technology, submitted*.

Wahyudie, A., Jama, M., Saeed, O., Noura, H., Assi, A., and Harib, K. (2015). Robust and low computational cost controller for improving captured power in heaving wave energy converters. *Renewable Energy*, 82, 114–124.